THE ASTROPHYSICAL JOURNAL, 535:615–620, 2000 June 1
© 2000. The American Astronomical Society. All rights reserved. Printed in U.S.A.

EXTREME ULTRAVIOLET EXPLORER OBSERVATIONS OF CLUSTERS OF GALAXIES: VIRGO AND M87

THOMAS W. BERGHÖFER,[1,2] STUART BOWYER,[1] AND ERIC KORPELA[1]
Received 1999 August 24; accepted 2000 January 12

ABSTRACT

We present results of a reanalysis of archival *Extreme Ultraviolet Explorer* (*EUVE*) data of the central region of the Virgo Cluster. We employ the new analysis method developed by Bowyer, Berghöfer, & Korpela and find diffuse emission reaching out to a distance of $\approx 13'$. The spatial distribution of this flux is incompatible with a thermal plasma origin. We investigate whether this emission is due to inverse Compton scattering of relativistic electrons against the 3 K blackbody background. We show that this emission cannot be produced by an extrapolation to lower energies of the observed synchrotron radio-emitting electrons, and an additional component of low-energy relativistic electrons is required. In addition to discussing the diffuse EUV emission, we present an analysis of the EUV emission originating from the jet in M87.

Subject headings: galaxies: clusters: individual (Virgo) — intergalactic medium — ultraviolet: galaxies

1. INTRODUCTION

Observations with the *Extreme Ultraviolet Explorer* (*EUVE*) have provided evidence that a number of clusters of galaxies produce intense EUV emission (e.g., Bowyer, Lieu, & Mittaz 1997). The initial explanation for this emission was that it is produced by a diffuse, $(5–10) \times 10^5$ K thermal gas component of the intracluster medium (ICM). Gas at these temperatures cools very rapidly, however, and there is no obvious energy source to reheat it (Fabian 1996). Consequently, a number of other mechanisms have been investigated as the source of the emission. Inverse Compton (IC) scattering of cosmic microwave background photons by relativistic electrons present in the ICM was proposed as the source of the observed EUV emission in the Coma Cluster (Hwang 1997; Ensslin & Biermann 1998). However, Bowyer & Berghöfer (1998) have shown that the spatial distribution of the EUV emission in this cluster is not consistent with IC emission from the observed population of relativistic electrons.

A variety of alternative explanations have been advanced that dismiss the *EUVE* excess in clusters of galaxies. Most recently, Arabadjis & Bregman (1999) argue that the EUV excess can be explained away by a different cross section for absorption by hydrogen and helium in the foreground interstellar medium (ISM) column. Bowyer, Berghöfer, & Korpela (1999) find that in some clusters this may account for some of the excess present in the *ROSAT* Position Sensitive Proportional Counter (PSPC) data; however, this cannot explain the intense EUV excesses found with *EUVE*.

Bowyer et al. (1999) reexamined *EUVE* data of the clusters Abell 1795, Abell 2199, and Coma. They demonstrated that the initially reported results are based on an improper background subtraction. In previous analyses a flat background had been assumed. However, a detailed investigation of blank field observations with the *EUVE* Deep Survey (DS) instrument shows that the background consists of two independent components, a nonphotonic background and a background due to photons. The nonphotonic background level can be determined in obscured regions of the detector and can be directly subtracted from the raw data. However, the photonic background is affected by telescope vignetting and must be treated differently.

In the case of Abell 1795 and Abell 2199, Bowyer et al. (1999) show that the extent of the diffuse EUV emission is much smaller than earlier reported. Furthermore, the radial EUV emission profiles of these two clusters show a flux deficit compared to the soft energy tail of the X-ray–emitting intracluster gas. These findings are consistent with the presence of strong cooling flows in Abell 1795 and Abell 2199.

In this paper we employ our new reduction method to *EUVE* archival data of the central part of the Virgo Cluster. We compare our results with results derived from radio observations of this region. We consider the possibility that the observed diffuse EUV excess emission is due to an inverse Compton process of the known population of relativistic electrons in the ICM near M87. Furthermore, we investigate the emission originating from the jet in M87 and compare our results with observations at other wavelengths.

2. DATA AND DATA ANALYSIS

The Virgo Cluster has been observed for 36,000 s with the Deep Survey (DS) telescope of *EUVE* (Bowyer & Malina 1991). Data reduction was carried out with the *EUVE* package built into IRAF, which is especially designed to process *EUVE* data.

In order to reduce the nonphotonic (nonastronomical) background contribution to the data, we investigated the pulse-height spectrum of all detected events. A large number of *EUVE* DS observations of all kinds of astronomical targets has shown that a typical pulse-height spectrum consists of two components, a Gaussian profile representing the source events and an exponential background distribution. More details about the different background contributions to the DS data and the method of pulse-height thresholding can be found in Berghöfer et al. (1998). From our experience with stellar and extragalactic observations with *EUVE* we know that the pulse-height selection effectively reduces the nonastronomical back-

[1] Space Sciences Laboratory, University of California, Berkeley, CA 94720-7450.
[2] Hamburger Sternwarte, Universität Hamburg, Gojenbergsweg 112, D-21029, Hamburg, Germany.

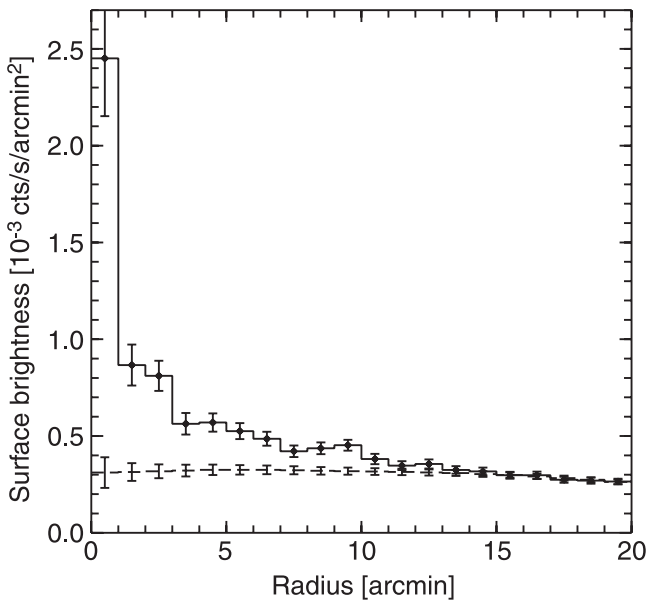

FIG. 1.—Azimuthally averaged radial intensity profile of the EUV emission in the central part of Virgo (centered on M87), shown as a solid line. The dashed line is the vignetted background. There is no EUV emission beyond $i \approx 13'$.

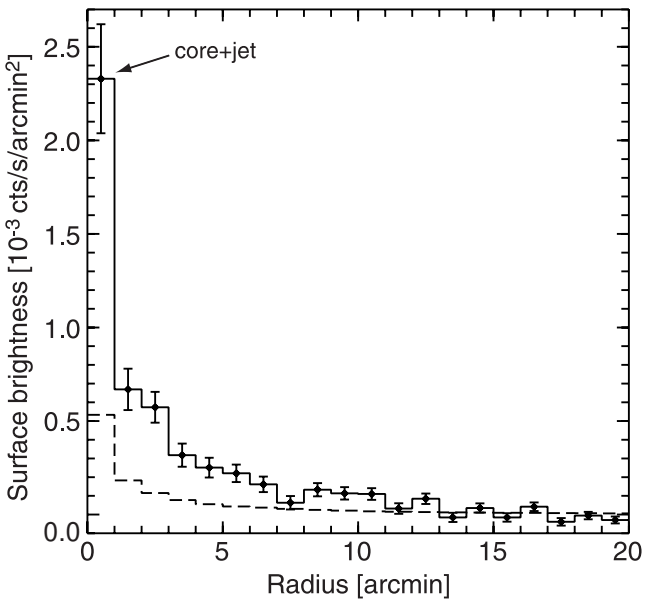

FIG. 2.—Azimuthally averaged radial intensity profile of the background-subtracted EUV emission in the central part of Virgo, shown as a solid line. The dashed line provides the contribution of the low-energy tail of the X-ray–emitting intracluster gas. The central 1′ bin is dominated by the core and jet in M87 and must be ignored in the context of diffuse emission.

ground in the data without any significant reduction of the source signal. By comparing the source signal with and without pulse-height selection, we find that the effect on the source signal is lower than 4%.

Then we applied corrections for detector dead time and for telemetry limitations (Primbsching) to the screened event list and produced a DS EUV image of the Virgo Cluster. We then determined the nonphotonic background level in the image from highly obscured regions at the outermost parts of the field of view near the Lexan/B filter frame bars. This nonastronomical background contribution is assumed to be constant over the entire detector field and was subtracted from the image.

In order to subtract the (vignetted) photonic background, we computed the azimuthally averaged radial emission profile centered on M87. We used the *EUVE* DS sensitivity map provided by Bowyer et al. (1999) to determine a radial sensitivity profile centered on the detector position of M87. This was then fitted to the outer part (15′–20′) of the radial emission profile to determine the scaling factor between sensitivity profile and the photonic background in the data. The radial emission profile and the best-fit background model are shown in Figure 1.

3. RESULTS

The data in Figure 1 demonstrate the presence of diffuse EUV emission in the vicinity of M87 which extends to a radius of $\approx 13'$. At larger radii the radial profile is well fitted by the background model, demonstrating the absence of any significant cluster emission beyond this. The initial publication on the diffuse EUV emission from Virgo (Lieu et al. 1996) claimed to detect excess emission to 20′.

In Figure 2 we plot the background-subtracted radial EUV emission profile (*solid line*). The dashed line shows the expected EUV emission of the low-energy tail of the X-ray–emitting diffuse intracluster gas as derived in the following. Note that the inner 1′ bin is dominated by the core and jet of M87 and must be ignored for the discussion of the diffuse emission.

To determine the diffuse X-ray contribution to the observed EUV emission, we processed *ROSAT* PSPC archival data of the Virgo Cluster. We used standard procedures implemented in the EXSAS software package to produce an image from the photon event list. Then a vignetting-corrected exposure map was computed for this data set and a PSPC count-rate image was generated by dividing the PSPC image by the exposure map.

We point out that the background in the *ROSAT* PSPC hard energy band is dominated by the photonic (vignetted) background, and the contribution of the nonphotonic background is minor. Therefore, an analysis similar to that described for the *EUVE* DS data including a separation of the photonic and nonphotonic background contributions is not essential. However, in the case of detectors with low effective areas (e.g., *BeppoSAX*), and less efficient rejection mechanisms for nonphotonic events, this background contribution must be treated separately.

For our analysis of the *ROSAT* PSPC data we selected only photon events in the hardest energy band, channels 90–236. This channel selection has several advantages. First, any contamination by a possible steep-spectrum source at soft X-ray energies is excluded and, therefore, ensures that this bandpass represents only thermal contributions to the overall diffuse emission in Virgo. Second, this part of the *ROSAT* band pass is nearly unaffected by interstellar absorption. This minimizes errors due to possible differential ISM absorption effects when modeling conversion factors between DS and PSPC counts. Third, the count-rate conversion factor between DS and PSPC is nearly temperature independent in the range of X-ray temperatures measured in the central Virgo region and, thus, *ROSAT* count rates of the diffuse X-ray emission can be

converted into DS count rates by using one single conversion factor.

In order to be able to convert PSPC counts into DS counts, we modeled conversion factors for a range of plasma temperatures (0.1–2.7 keV) employing the MEKAL plasma emission code with abundances of 0.34 solar (Hwang et al. 1997). These calculations include absorption by the interstellar medium. We used an ISM absorption column density of 1.72×10^{20} cm^{-2} (Hartmann & Burton 1997) and an absorption model including cross sections and ionization ratios for the ISM as described in Bowyer et al. (1999). In Figure 3 we show the DS-to-PSPC count-rate conversion factor. The left-hand scale and the solid curve give the plasma temperature as a function of the DS-to-PSPC count-rate ratio. As can be seen, for a wide range of temperatures (0.6–2.7 keV) the model conversion factor is constant within 15%. According to Böhringer et al. (1995) and Böhringer (1999), the temperature of the X-ray–emitting intracluster gas in the Virgo Cluster is $\approx$2 keV. In addition to this thermal gas component, these authors detected several diffuse emission features near M87 that are significantly softer than the average Virgo Cluster gas temperature. However, spectral fits to the *ROSAT* data do not provide any evidence for gas at temperatures below 1 keV (H. Böhringer 1999, private communication). For temperatures near 1 keV the modeled conversion factor for a thermal gas is slightly lower than for higher temperatures. Therefore, the contribution of the lower temperature components to the overall diffuse X-ray emission in the EUV bandpass is lower than the dominant 2 keV cluster gas component. Using the conversion factor appropriate for the mean cluster gas temperature of 2 keV for the entire emission, including the softer thermal enhancements, slightly overestimates the low-energy X-ray contribution to the EUV emission.

We also modeled the DS-to-PSPC conversion factor for a nonthermal power-law type spectrum including ISM absorption. The right-hand scale and dashed curve give the power-law spectral index as a function of the modeled conversion factor.

In Figure 4 we show the observed ratio between azimuthally averaged radial intensity profiles observed with the *EUVE* DS and PSPC. Within the error bars the ratio is constant (reduced $\chi^2 = 0.9$). The best-fit value is 0.0186 ± 0.0057. The ratio for the inner 1′ bin is consistent with this value; however, we excluded this point because of the presence of emission from the core and jet of M87. Sarazin & Lieu (1998) have suggested that an increasing EUV–to X-ray–emission ratio toward larger distances from the cluster center is an indication of an inverse Compton process producing the EUV emission in the cluster. However, the data in Figure 4 demonstrate that this is not observed in the central Virgo region.

Our best-fit value of 0.0186 is $\approx$4.3 times larger than expected for the low-energy tail of the X-ray–emitting gas in the Virgo Cluster. Therefore, the X-ray contribution to the observed EUV excess in the central part of the Virgo Cluster must be minor.

It is clear that the ratio between observed EUV flux and modeled X-ray contribution cannot be used directly to determine the physical parameters of the source. Instead, one must first subtract the X-ray contribution from the observed EUV emission.

In Figure 5 we show the spatial distribution of the EUV excess emission in the central Virgo region; the background and the contribution of the low-energy tail of the X-ray–emitting ICM have been subtracted. The central emission peak at the position of M87 is surrounded by a diffuse EUV emission structure which is asymmetric in shape. Its extent varies between 1′ and 7′. Several armlike features are visible. At larger radii the EUV emission results from a number of apparently discrete and extended diffuse features in the M87 radio halo region. These emission features are consistent with the emission seen in the surface brightness profile (Fig. 2) between 9′ and 13′. These asymmetric features show that the flux is not produced by a gravitationally bound thermal

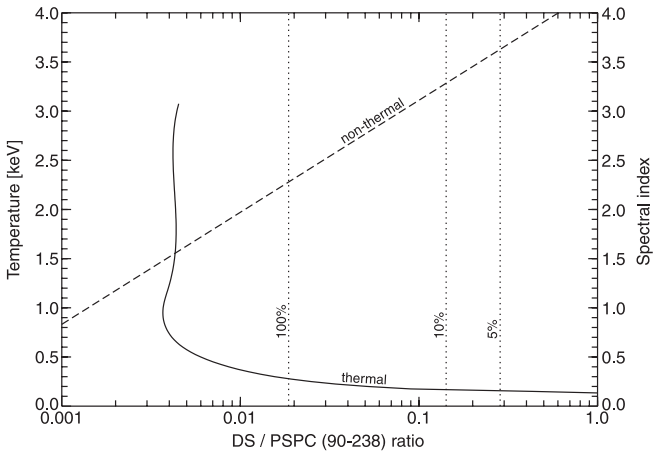

FIG. 3.—Conversion factors from *ROSAT* PSPC count rates into *EUVE* DS rates modeled for a spectrum of a thermal plasma model and a nonthermal power-law type source including the ISM absorption toward the Virgo Cluster. *Ordinates:* Left-hand scale and solid curve give the plasma temperature for the thermal model; right-hand scale and dashed curve give the power-law spectral index for the nonthermal model. Three dotted vertical lines, labeled with 100%, 10%, and 5%, indicate relative contributions of the hard energy tail of the EUV excess component to the overall X-ray emission in the analyzed *ROSAT* band (see § 4.1).

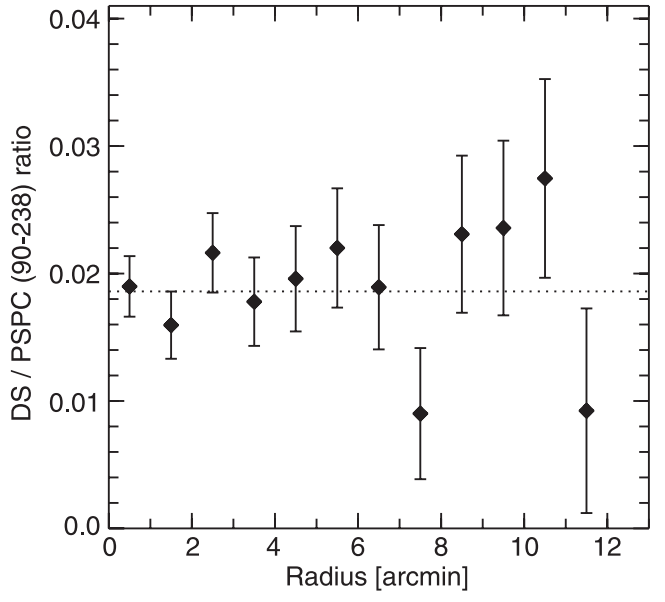

FIG. 4.—Ratio between observed azimuthally averaged intensity profiles observed with the *EUVE* DS and the *ROSAT* PSPC. The dotted line represents the best-fit value of 0.186 assuming a constant ratio.

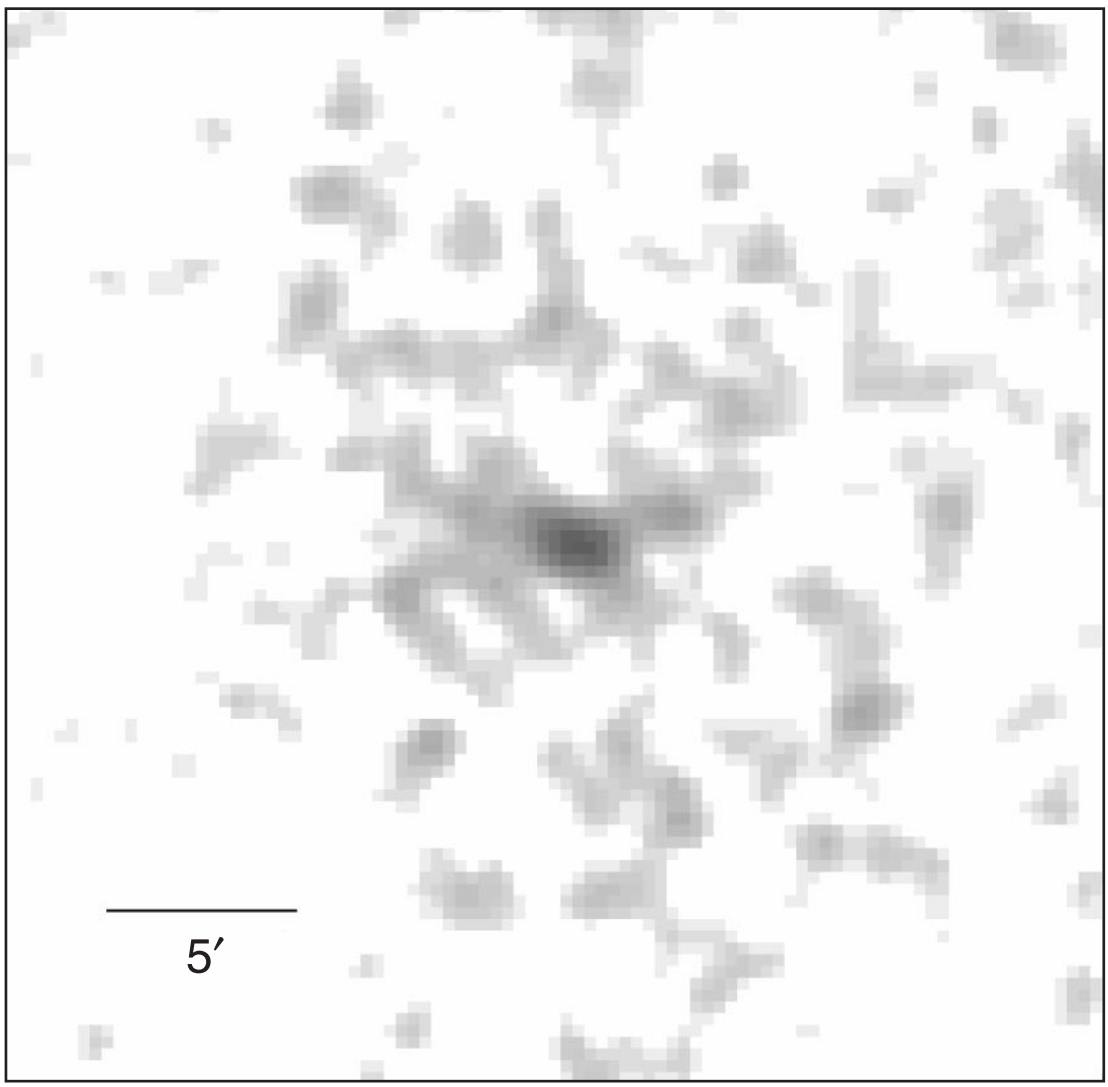

FIG. 5.—Spatial distribution of the EUV excess emission in the central Virgo region. The contribution of the low-energy tail of the X-ray–emitting ICM has been subtracted from the data.

gas. For the diffuse EUV emission within 7′ (excluding the core + jet emission in the inner 1′), we determine a total count rate of 0.036 ± 0.006 counts s^{-1}. Assuming an extraction radius of 13′ results in a total count rate of 0.066 ± 0.009 counts s^{-1}.

We also investigated the EUV emission peak at the position of M87. X-ray observations with the *Einstein* and *ROSAT* HRIs have demonstrated that the central X-ray emission peak splits into two major components, which are associated with the core and mainly knots A + B + C of the jet in M87. The spatial resolution of the *EUVE* DS ($\approx 20''$) is not sufficient to completely resolve the jet from the galaxy core. However, the central peak indicates emission slightly elongated by about one resolution element in the direction from the core to the jet. The central emission peak (core + jet) provides a total count rate of $(4.9 \pm 0.6) \times 10^{-3}$ counts s^{-1} in excess of the diffuse emission component.

4. DISCUSSION AND CONCLUSIONS

4.1. *Diffuse EUV Emission*

The results of our reanalysis show a clear EUV excess in the central Virgo region around M87. Compared to previous studies the azimuthally averaged extent of this emission is smaller and extends only to $\approx 13'$ from the center of M87.

To explore the nature of the EUV excess, we compare this emission with a 90 cm radio map of the central Virgo region near M87 (Owen, Eilek, & Kassim 1999). If the diffuse EUV emission is due to inverse Compton processes in the ICM, one would expect to see similar emission features in both the EUV and radio image. In Figure 6 we show a contour plot of the EUV emission superposed on the 90 cm radio map. As can be seen, the EUV emission peaks at the position of the radio emission of the core and jet of M87. EUV excess emission features are, however, not directly coincident with any of the other brighter features visible in the radio map. The EUV emission is also not associated with the higher temperature X-ray emission features seen in the *ROSAT* PSPC images in Virgo (see Böhringer 1999; Harris et al. 1999).

We next investigate whether the integrated flux of the diffuse EUV emission is compatible with an inverse Compton origin of the observed EUV excess in the central Virgo region. We use the observed radio synchrotron power-law spectrum of the M87 halo ($\alpha = 0.84$; Herbig &

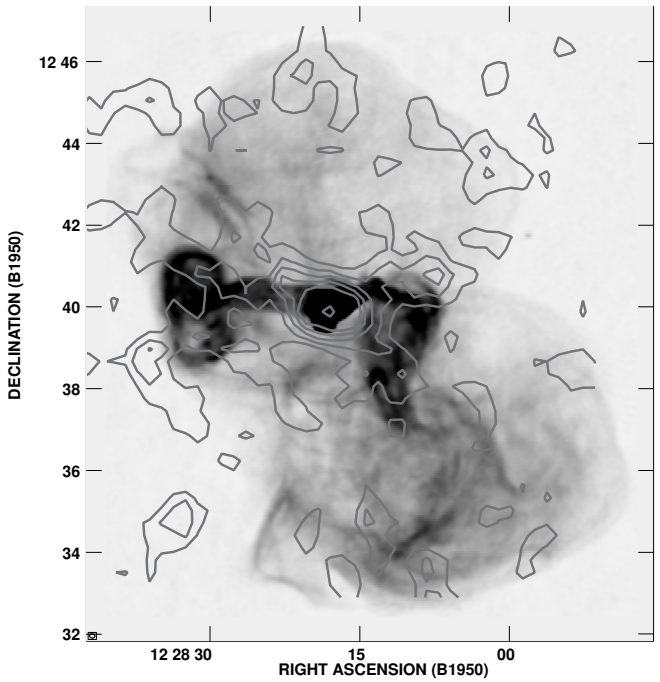

FIG. 6.—Contour plot of the background and X-ray–subtracted EUV emission shown superposed on the 90 cm radio map of the M87 halo. The contours provide fluxes of 1.5, 4.5, 7, 10, 13, and 27 σ above the noise level.

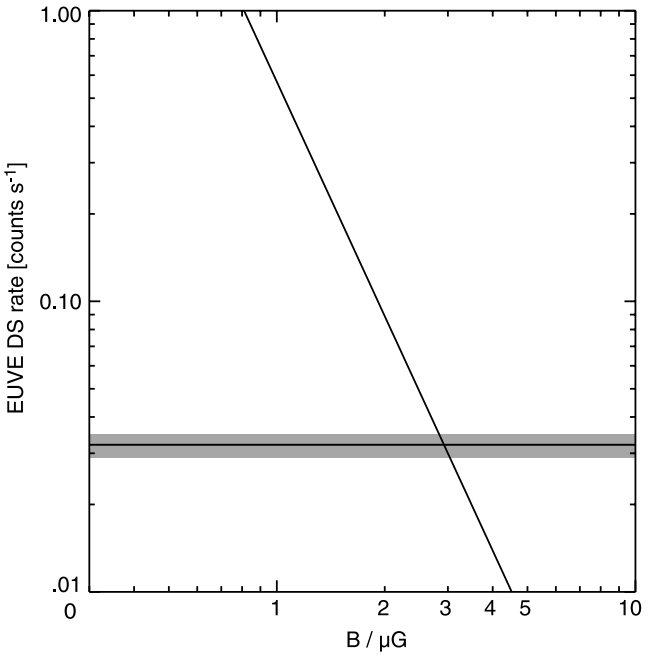

FIG. 7.—*EUVE* DS count rate as a function of magnetic field strength. The horizontal line provides the observed total count rate for the diffuse emission component. The error in this value is shown as a gray shaded area.

Readhead 1992) to compute the underlying distribution of relativistic electrons in this region and its inverse Compton flux. Note that the radio spectrum needs to be extrapolated into the low-frequency range near 1 MHz, which is not observable because of ionospheric effects. The conversion from the synchrotron spectrum into an electron energy distribution depends on the magnetic field strength in the ICM. We derive a relation between magnetic field strength and the inverse Compton flux produced by the relativistic electrons; the results are shown in Figure 7. The flux is folded with the *EUVE* DS response and given in units of DS counts s^{-1}, which allows a direct comparison to the observed integrated DS count rate of the diffuse emission (Fig. 7, *horizontal line*). As can be seen, for a magnetic field strength of ≈ 3 μG the observed flux matches the model flux. Note that this value would also be consistent with Faraday rotation measurements in the M87 halo (Dennison 1980).

However, with $\alpha = 0.84$ the radio synchrotron spectrum is inconsistent with the required steep EUV to X-ray power-law spectrum. In Figure 3 we show three dotted vertical lines labeled 100%, 10%, and 5%. These lines indicate relative contributions of the hard energy tail of the EUV excess component to the overall X-ray emission in the *ROSAT* band. A contribution of 100% is obviously not realistic since this would require that no emission is seen from the gravitationally bound intracluster gas. The other two dotted lines show 10% and 5% contributions, respectively. No other emission component in excess of the thermal component has been detected in the *ROSAT* PSPC data of Virgo, and only an upper limit can be derived from these data. A determination of an accurate upper limit for the EUV excess component in the *ROSAT* band is highly model dependent. However, from our experience with *ROSAT* data of diffuse sources we estimate that a contribution of 10% should be detectable. If we assume a 10% contribution as the upper limit for the EUV excess component in the *ROSAT* band, according to Figure 3 a power-law photon number index of $\alpha \geq 3.2$ is required to explain the observed EUV flux and the upper limit in the *ROSAT* PSPC hard band (channels 90–238) by a nonthermal power-law source. Therefore, inverse Compton emission from the known population of relativistic electrons in the M87 halo cannot account for the observed EUV excess in the central Virgo region.

We compute the total luminosity of the diffuse EUV emission for a steep nonthermal power-law spectrum and for a low-temperature thermal plasma spectrum, since these have been discussed in the literature, but we make no claim that either of these is the correct spectral distribution for the emission. Assuming a power-law spectrum with $\alpha = 3.2$ results in a luminosity of 5.2×10^{42} ergs s^{-1} in the 0.05–0.2 keV band. For a thermal plasma with a temperature of 0.15 keV we obtain a luminosity of 5.7×10^{42} ergs s^{-1}. These values were derived from the total count rate of the diffuse EUV emission within 7′. Including the apparently discrete and extended diffuse EUV emission detected between 7′ and 13′ increases the luminosity by 80%. Assuming larger power-law indices or lower plasma temperatures result in higher luminosities. For the luminosity calculations we assume a distance of 17 Mpc.

4.2. *EUV Emission of the Jet in M87*

Since the core and jet of M87 cannot be resolved in the *EUVE* image of M87, we assume that the X-ray flux ratio between core and jet that can be determined from the *ROSAT* HRI observations is also valid for the EUV fluxes. Harris, Biretta, & Junor (1997) give a ratio of ≈ 1.5 for the core/jet X-ray flux ratio. Based on their compilation of measurements for the jet in M87, Meisenheimer, Röser, &

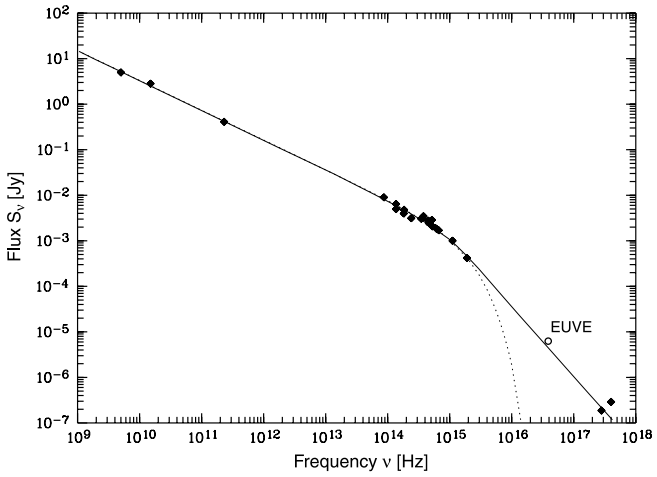

FIG. 8.—Radio to X-ray spectrum of the jet in M87 The solid line shows the model provided by Meisenheimer et al. (1996). The *EUVE* data point is well fitted by this model with a cutoff at UV wavelengths.

Schlötelburg (1996) derived a spectral index of 0.65 for the radio to near-UV spectrum. In order to be able to explain the X-ray emission of the jet in M87 by the same spectrum, these authors introduced a spectral cutoff near 10^{15} Hz. The spectral index of the UV to X-ray power-law spectrum then has to be $\alpha \approx 1.4$ to explain the UV and X-ray data.

Based on these assumptions, we compute a flux of 3.4×10^{-12} ergs cm^{-2} s^{-1} (6.5×10^{-6} Jy) and a luminosity of 1.2×10^{41} ergs s^{-1} for the emission of the M87 jet in the *EUVE* DS bandpass. For the luminosity calculation we assume a distance of 17 Mpc.

In Figure 8 we show the radio to X-ray spectrum of the jet in M87 including the *EUVE* data point. As can be seen, the spectral model provided by Meisenheimer et al. (1996) also fits the *EUVE* observations. This confirms the suggested cutoff in the UV and further supports the conclusion that the entire jet emission, from the radio to the X-ray band, is synchrotron radiation produced by relativistic electrons in the jet.

5. SUMMARY

The observed EUV excess in the central Virgo region is not spatially coincident with either the distribution of the radio emission or the observed high-temperature thermal X-ray emission seen in the *ROSAT* images. This provides strong evidence that a separate source mechanism is present. In addition, because of the required steep EUV to X-ray spectrum, this emission cannot be produced by an extrapolation to lower energies of the observed synchrotron radio-emitting electrons. If the observed EUV excess is inverse Compton emission, a new population of relativistic electrons is required. Therefore, the same difficulties as in the case of the explanation of the EUV excess of the Coma Cluster (see Bowyer & Berghöfer 1998) exist in the central Virgo region. The *EUVE* observations of M87 are consistent with the spectral cutoff in the spectrum of the jet in M87 as suggested by Meisenheimer et al. (1996). This further supports the idea that the EUV and X-ray emission of the jet is synchrotron radiation.

We thank Jean Eilek for providing us a postscript file of the M87 radio map. We acknowledge useful discussions with John Vallerga, Jean Dupuis, and Hans Böhringer. This work was supported in part by NASA contract NAS5-30180. T. W.B. was supported in part by a Feodor-Lynen Fellowship of the Alexander–von-Humboldt-Stiftung.

REFERENCES

Arabadjis, J. S., & Bregman, J. N. 1999, ApJ, 514, 607
Berghöfer, T. W., Bowyer, S., Lieu, R., & Knude, J. 1998, ApJ, 500, 838
Böhringer, H. 1999, in Diffuse Thermal and Relativistic Plasma in Galaxy Clusters, ed. H. Böhringer, L. Feretti, & P. Schuecker (MPE Rep. 271; Garching: MPE), 115
Böhringer, H., Nulsen, P. E. J., Braun, R., & Fabian, A. C. 1995, MNRAS, 274, L67
Bowyer, S., & Berghöfer, T. W. 1998, ApJ, 506, 502
Bowyer, S., Berghöfer, T. W., & Korpela, E. 1999, ApJ, 526, 592
Bowyer, S., Lieu, R., & Mittaz, J. P. 1997, in IAU Symp. 188, The Hot Universe, ed. K. Koyama, S. Kitamoto, & M. Hoh (Dordrecht: Kluwer), 52
Bowyer, S., & Malina, R. F. 1991, in Extreme Ultraviolet Astronomy, ed. R. F. Malina & S. Bowyer (New York: Pergamon), 397
Dennison, B. 1980, ApJ, 236, 761
Ensslin, T., & Biermann, P. 1998, A&A, 330, 90
Fabian, A. C. 1996, Science, 271, 1244
Harris, D. E., Biretta, J. A., & Junor, W. 1997, MNRAS, 284, L21
Harris, D. E., Owen, F., Biretta, J. A., & Junor, W. 1999, in Diffuse Thermal and Relativistic Plasma in Galaxy Clusters, ed. H. Böhringer, L. Feretti, & P. Schuecker (MPE Rep. 271; Garching: MPE), 111
Hartmann, D., & Burton, W. B. 1997, Atlas of Galactic Neutral Hydrogen (Cambridge: Cambridge Univ. Press)
Herbig, T., & Readhead, A. C. S. 1992, ApJS, 81, 83
Hwang, C.-Y. 1997, Science, 278, 1917
Hwang, U., Mushotzky, R. F., Loewenstein, M., Markert, T. H., Fukuzawa, Y., & Matsumoto, H. 1997, ApJ, 476, 560
Lieu, R., et al. 1996, ApJ, 458, L5
Meisenheimer, K., Röser, H.-J., & Schlötelburg, M. 1996, A&A, 307, 61
Owen, F., Eilek, J., & Kassim, N. 1999, Diffuse Thermal and Relativistic Plasma in Galaxy Clusters, ed. H. Böhringer, L. Feretti, & P. Schuecker (MPE Rep. 271; Garching: MPE), 107
Sarazin, C., & Lieu, R. 1998, ApJ, 494, L177